Title

Phonon-Driven Femtosecond Dynamics of Excitons in Crystalline Pentacene from First Principles

Journal

Physical Review Letters, 132(12)

ISSN

0031-9007

Authors

Cohen, Galit

Haber, Jonah B

Neaton, Jeffrey B

et al.

Publication Date

2024-03-22

DOI

10.1103/physrevlett.132.126902

Phonon-Driven Femtosecond Dynamics of Excitons in Crystalline Pentacene from First Principles

Galit Cohen,[1] Jonah B. Haber,[2,3] Jeffrey B. Neaton,[2,3,4] Diana Y. Qiu,[5,*] and Sivan Refaely-Abramson[1,†]

[1]*Department of Molecular Chemistry and Materials Science, Weizmann Institute of Science, Rehovot 7610001, Israel*

[2]*Department of Physics, University of California Berkeley, Berkeley, California 94720, USA*

[3]*Materials Sciences Division, Lawrence Berkeley National Laboratory, Berkeley, California 94720, USA*

[4]*Kavli Energy Nanosciences Institute at Berkeley, Berkeley, California 94720, USA*

[5]*Department of Mechanical Engineering and Materials Science, Yale University, New Haven, Connecticut 06520, USA*

(

Nonradiative exciton relaxation processes are critical for energy transduction and transport in optoelectronic materials, but how these processes are connected to the underlying crystal structure and the associated electron, exciton, and phonon band structures, as well as the interactions of all these particles, is challenging to understand. Here, we present a first-principles study of exciton-phonon relaxation pathways in pentacene, a paradigmatic molecular crystal and optoelectronic semiconductor. We compute the momentum- and band-resolved exciton-phonon interactions, and use them to analyze key scattering channels. We find that both exciton intraband scattering and interband scattering to parity-forbidden dark states occur on the same ∼100 fs timescale as a direct consequence of the longitudinal-transverse splitting of the bright exciton band. Consequently, exciton-phonon scattering exists as a dominant nonradiative relaxation channel in pentacene. We further show how the propagation of an exciton wave packet is connected with crystal anisotropy, which gives rise to the longitudinal-transverse exciton splitting and concomitant anisotropic exciton and phonon dispersions. Our results provide a framework for understanding the role of exciton-phonon interactions in exciton nonradiative lifetimes in molecular crystals and beyond.

Molecular crystals are broadly used as host systems for energy transfer processes involving energetically excited states in which excitons—bound electron and hole pairs—serve as the main energy carriers [1,2]. The light harvesting efficiency in these materials depends on exciton relaxation and mobility and the dynamical processes they stem from. Well-explored examples are the acene-based crystals [3], especially pentacene, for which spectroscopic and microscopic measurements reveal unique nonradiative decay channels [4,5]. These decay processes are associated with optically forbidden states due to spin, parity, and momentum. Long exciton lifetimes up to the order of nanoseconds, associated with nonradiative relaxation processes, have been reported [6–10], and the change in the spatiotemporal shape of the propagating light excitation, as seen in transient microscopy experiments [11,12], reveals anisotropic transport signatures, reflecting the underlying crystal packing [5,13].

In solid pentacene, recent first-principles calculations predicted two nearly degenerate, low-lying singlet excitons, one bright of even parity and another dark of odd parity [14,15]. Such optical selection rules exist due to the presence of inversion symmetry, and the relative energies of these two exciton bands are dictated by the molecular monomers and their packing arrangement. Coherent transitions between these singlet states and bitriplets [14,16] allow the so-called "singlet fission" process, greatly increasing photovoltaic efficiency [7,17]. Pentacene crystal anisotropy also gives rise to a longitudinal-transverse (LT) splitting of the bright exciton branches, recently connected to ultrafast anisotropic exciton transport in the short-time quasiballistic regime, prior to thermalization [18]. This LT splitting results in the bright exciton branch straddling the energy of the dark exciton branch, making the manifold of bright and dark states (and hence the scattering between them) exceptionally complex. It is of great interest to understand the role of exciton LT splitting in exciton-phonon interactions, phonon-mediated relaxation channels, and the occupation of long-lived states involved in nonradiative processes such as singlet fission as well as in anisotropic transport phenomena.

Understanding exciton-phonon scattering in molecular crystals requires a quantitatively predictive, structure-sensitive theoretical analysis that treats electron-hole and electron-phonon coupling on the same footing. Given that the envelope function of optical excitations in these systems can span over several nanometers [19–21], crystal effects are significant [22–27]. Density functional theory (DFT) [28] allows accurate calculations of the ground state. The *GW* approach [29] within many-body perturbation theory

supplies reliable quasiparticle band structures, and excitons are calculated within the *GW* plus Bethe-Salpeter equation (*GW*-BSE) approach [15,20,30–35], including finite momentum exciton states [14,36–38]. These are essential in exciton dynamics upon coupling to phonons. Density functional perturbation theory (DFPT) [39] or finite-displacement methods [40,41] provide accurate phonon dispersion and electron-phonon scattering matrix elements. However, treating exciton-phonon interactions on an equivalent footing is extremely challenging and the theoretical development of which is still nascent. Recent advances allow computations of exciton-phonon self energies within many-body perturbation theory [42–47], but such techniques have not been applied to molecular crystals, in part due to their structural complexity. While recent work established how phonons renormalize excitation energies [48], the role of exciton-phonon scattering in relaxation dynamics and transport in these systems is yet to be explored.

In this Letter, we present a first-principles approach to study phonon-induced exciton dynamics, applied to crystal pentacene. We explore exciton intraband and interband transitions and their role in the early stages of exciton transport and ultrafast occupation of long-lived dark states. We compute exciton-phonon interactions by treating the electron-hole and electron-phonon coupling to the same level of theory within many-body perturbation theory. Electron-hole interactions are calculated from *GW*-BSE [30,49], with exciton-phonon self-energy on top of it [45,50]. This is necessary to obtain quantitatively accurate exciton-phonon interactions, identify key exciton relaxation channels, and predict ultrafast state evolution upon photoexcitation, and in particular the interplay between intraband scattering and interband decay into a dark state. Interestingly, we find that these two processes have comparable timescales, a consequence of the exciton LT splitting and the bright and dark exciton state crossing. Moreover, the exciton wave packet delocalizes rapidly and anisotropically in a bandlike transport regime, a result of the integrated exciton-phonon coupling and LT splitting. Our findings provide theoretical understanding of the structurally tunable phonon scattering in pentacene, involved already at very early stages of exciton transport and manifested in anisotropic exciton wave packet spreading proceeding long-lived dark state occupation, as observed in recent experiments [5,13,51–53].

We study crystalline pentacene in its bulk phase [54], with a herringbone structure of Van der Waals-stacked molecules, as shown in Fig. 1(a). Exciton states are computed from *GW*-BSE on top of a ground state obtained from DFT [49]. The exciton band structure is calculated by solving the BSE for electrons and holes with different momenta [36] [see Supplemental Material [55] (SM) for full details]. Figure 1(b) shows the exciton band structure of the two lowest singlet exciton states. Ω_S is the excitation

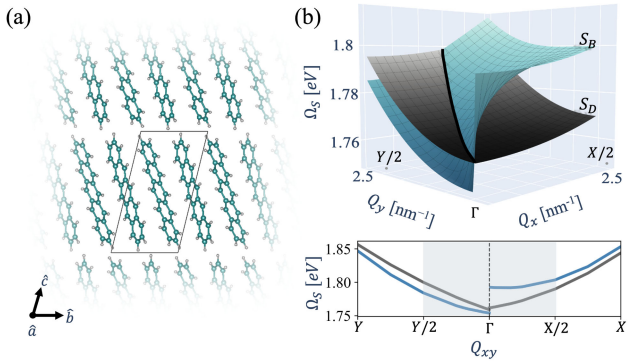

FIG. 1. (a) Atomic structure of pentacene crystal (carbon and hydrogen in teal and gray, respectively). (b) Top: exciton band structure of the low-lying bright (S_B, blue) and dark (S_D, black) singlet excitons interpolated from the computed *GW*-BSE exciton dispersion along the reciprocal $\hat{\mathbf{a}}$-$\hat{\mathbf{b}}$ plane of the Brillouin zone. A longitudinal-transverse splitting of the bright state at Γ results in band intersection of the two states (black line). Bottom: the exciton band structure along the $Y-\Gamma-X$ k path (in crystal coordinates, shaded area marks the region displayed in the top panel).

energy of exciton S, for electrons and holes with momentum difference $\mathbf{Q}_{x,y}$ at the $\hat{\mathbf{x}}$, $\hat{\mathbf{y}}$ directions. At $\mathbf{Q}=\Gamma$ the two low-lying singlet excitons are of opposite parities, one optically bright (S_B, blue) and the second optically dark (S_D, black). Importantly, the bright state exhibits a characteristic LT splitting at the Γ point arising from long-range exchange interaction [18], previously explored analytically [63–65]. This property introduces an angular dependency in the relative energy alignment between the bands, where the bright state has a higher (along $\Gamma-X$) or lower (along $\Gamma-Y$) excitation energy than the dark state. Therefore, transitions between the bright and the dark states are expected to depend anisotropically on the exciton-phonon scattering.

Phonon modes are computed using DFPT, where the change in the DFT Kohn-Sham potential upon phonon displacement is evaluated explicitly [39] for lattice vectors fixed to the experimental values and internally relaxed, a procedure shown to supply reliable phonons in organic crystals [66] (see SM [55]). We combine the computed phonon and exciton states to evaluate the exciton-phonon scattering matrix elements [42,45]:

$$\mathcal{G}_{SS'\nu}(\mathbf{Q},\mathbf{q}) = \sum_{vcc'\mathbf{k}} [A^{S\mathbf{Q}+\mathbf{q}}_{vc\mathbf{k}}]^* g_{cc'\nu}(\mathbf{k}+\mathbf{Q},\mathbf{q}) A^{S'\mathbf{Q}}_{vc'k} - \sum_{vv'c\mathbf{k}} [A^{S\mathbf{Q}+\mathbf{q}}_{vc\mathbf{k}}]^* g_{v'v\nu}(\mathbf{k},\mathbf{q}) A^{S'\mathbf{Q}}_{v'c\mathbf{k}+\mathbf{q}}, \quad (1)$$

where $\mathcal{G}_{SS'\nu}(\mathbf{Q},\mathbf{q})$ is the coupling between two *GW*-BSE exciton states, $|S(\mathbf{Q}+\mathbf{q})\rangle$ and $|S'(\mathbf{Q})\rangle$, via a phonon with momentum $\mathbf{q}$ and mode ν. $A^{S\mathbf{Q}}_{vc\mathbf{k}}$ are the amplitudes of v, c occupied (hole) and unoccupied (electron) states,

respectively, and $\mathbf{k}$ is the electronic wave vector. $g_{c'c\nu}$ and $g_{v'v\nu}$ are the electron-phonon and hole-phonon coupling terms, calculated with DFPT. The exciton-phonon scattering matrix elements can be used to construct the exciton-phonon self energy to first order [45,50], whose imaginary part gives the exciton-phonon scattering time [42,45]

$$\tau^{-1}_{SS'} = \frac{2\pi}{\hbar}\frac{1}{N_q N_Q}\sum_{\nu\mathbf{Qq}}|\mathcal{G}_{SS'\nu}(\mathbf{Q},\mathbf{q})|^2\rho(\Delta E_{SS'}(\mathbf{Q},\mathbf{q}) - \hbar\omega_{\mathbf{q}\nu}), \tag{2}$$

where N_q, N_Q are the number of grid points for phonon and exciton crystal momentum, respectively, and the density of states is

$$\begin{aligned}&\rho(\Delta E_{SS'}(\mathbf{Q},\mathbf{q}) - \hbar\omega_{\mathbf{q}\nu})\\ &= [(n_{\mathbf{q}\nu})\tilde{\rho}(\Omega_{S(\mathbf{Q})} - \Omega_{S'(\mathbf{Q}+\mathbf{q})} + \hbar\omega_{\mathbf{q}\nu})\\ &\quad + (1+n_{\mathbf{q}\nu})\tilde{\rho}(\Omega_{S(\mathbf{Q})} - \Omega_{S'(\mathbf{Q}+\mathbf{q})} - \hbar\omega_{\mathbf{q}\nu})].\end{aligned} \tag{3}$$

Here, $n_{\mathbf{q}\nu}$ is the phonon Bose-Einstein occupation function at temperature T, and we consider both phonon absorption and emission processes. $\tilde{\rho}$ are Gaussian distributions with broadening σ. We denote the weighted scattering rate for each transition with mode and momentum resolution by $k_{SS'\nu}(\mathbf{Q},\mathbf{q})$, so that the scattering time in Eq. (2) is re-expressed as $\tau^{-1}_{SS'} = N_q^{-1}N_Q^{-1}\sum_{\nu\mathbf{Qq}} k_{SS'\nu}(\mathbf{Q},\mathbf{q})$.

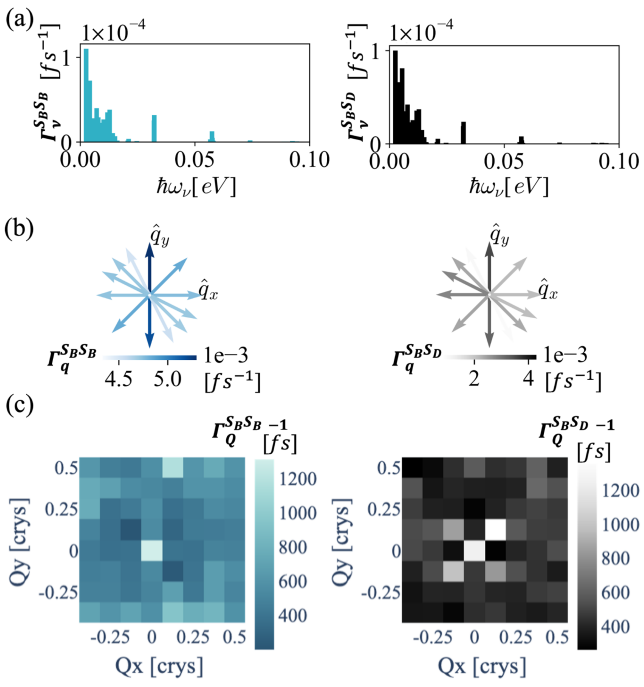

FIG. 2. Analysis of the computed exciton-phonon scattering for intraband (blue, left) and interband (black, right) transitions: (a) rates per phonon mode ν, (b) rates per phonon momentum $\mathbf{q}$, (c) scattering times per exciton momentum $\mathbf{Q}$.

Figure 2 shows the computed exciton-phonon scattering rates, for the two processes discussed above: intraband transitions from $S = S_B(\mathbf{Q})$ to $S' = S_B(\mathbf{Q}+\mathbf{q})$, namely within the optically bright state (blue, left); and interband transitions from $S = S_B(\mathbf{Q})$ to $S' = S_D(\mathbf{Q}+\mathbf{q})$, namely to the optically dark state (black, right). Figure 2(a) shows the scattering rates resolved over the phonon branch, $\Gamma^{SS'}_{\nu} = N_q^{-1}N_Q^{-1}\sum_{\mathbf{Qq}} k_{SS'\nu}(\mathbf{Q},\mathbf{q})$, plotted as a function of $\mathbf{q}$-averaged phonon energy, for $T = 300$ K and $\sigma = 0.02$ eV (this broadening parameter is compatible with grid spacing and energy differences between the exciton bands; see SM for further examination of temperature and broadening effects [55]). We observe dominance of low-frequency modes in both scattering channels. These include both acoustic and optical modes, and involve inter- and intramolecular vibrations. Intermolecular modes are coupled to delocalized low-lying singlet excitons, compared to localized excitons such as triplets that couple to intramolecular modes [25,26,67,68]. Figure 2(b) shows the scattering rates resolved per phonon momentum $\mathbf{q}$, $\Gamma^{SS'}_{\mathbf{q}} = N_Q^{-1}\sum_{\nu\mathbf{Q}} k_{SS'\nu}(\mathbf{Q},\mathbf{q})$. Arrows represent the phonon momentum direction and color stands for its associated rate, summed over all phonon modes and exciton momenta. Notably, we find larger contributions from phonons with momentum along the $\Gamma - Y$ direction, the transverse exciton direction, a property that plays an important role in the propagation dynamics examined below.

Figure 2(c) shows the inverse scattering rates per exciton crystal momentum $\mathbf{Q}$, where $\Gamma^{SS'}_{\mathbf{Q}} = N_q^{-1}\sum_{\nu\mathbf{q}} k_{SS'\nu}(\mathbf{Q},\mathbf{q})$. Square colors indicate the scattering times from $S_B(\mathbf{Q})$ to states in the same band with different momentum (left) and to the dark band S_D (right), summed over all momenta of the final exciton acquired due to the phonon momentum. The scattering times vary as a function of the initial exciton momentum, with weaker coupling around the Γ point. The total scattering times, as defined in Eq. (2), for the intraband and interband transitions are $\tau_{S_BS_B} \approx 500$ fs and $\tau_{S_BS_D} \approx 400$ fs, respectively. Both intraband and interband transitions are determined by scattering processes from multiple momentum states. Importantly, we find comparable scattering times between exciton intraband relaxation and the interband occupation of the dark state. This is robust upon increasing the number of participating bands and $\mathbf{k}$ grid (see SM [55]). This unexpected result suggests that the early stages of exciton evolution involve an interplay between two main relaxation pathways: intraband transitions due to phonon scattering, and interband transitions to a dark state. Such dark states are long-lived and expected to strongly couple with bitriplet excitons [14,69] that separate into triplet states, slowing down the exciton decay [5].

The rapid conversion of bright to dark states via phonon scattering is a clear consequence of the band crossing between these states due to the exciton LT splitting, with the band alignment determined from the molecular

components and packing. It can thus be tuned via crystal structure design. For example, in the case of tetracene, the bright exciton band is higher in energy and does not cross the dark band. Such band alignment results in prolonged scattering times, with interband scattering times larger than intraband ones by an order of magnitude (see SM [55]). We further emphasize that the matrix elements composing the scattering times shown in Fig. 2 for individual momentum channels span a large range in magnitude, including times as short as 30 fs for strongly coupled states and up to few 100 ps for weakly coupled ones, as demonstrated in Fig. S7 of the SM. This sets our results at competing timescales with coherent singlet-fission decay times in this system of ∼100 fs, yet faster than measured noncoherent processes at the order of nanoseconds [4,7,14,25,69].

To connect our calculations with experimental observations, we further study the effect of the computed intraband and interband scattering on a propagating exciton wave packet and its time-resolved evolution. The maximal computed exciton-phonon coupling in this system is few meV (see SM [55]), relatively weak compared to the exciton bandwidth of ∼100 meV. This supports perturbative treatment of the exciton scattering within a bandlike transport regime. We adopt a semiclassical kinetic equation form [56] (see derivation in the SM [55]) in which the time-resolved occupation of the bright exciton, $n_{S_B}(\mathbf{Q},\mathbf{R})$, is evaluated in both real ($\mathbf{R}$) and reciprocal ($\mathbf{Q}$) space through

$$\frac{\partial n_{S_B}(\mathbf{Q},\mathbf{R})}{\partial t} = -\frac{\partial n_{S_B}(\mathbf{Q},\mathbf{R})}{\partial x}\frac{\partial \Omega_{S_B}}{\partial \mathbf{Q}_x} - \frac{\partial n_{S_B}(\mathbf{Q},\mathbf{R})}{\partial y}\frac{\partial \Omega_{S_B}}{\partial \mathbf{Q}_y} + K_{\mathrm{scat}}[n_{S_B}(\mathbf{Q},\mathbf{R})]. \quad (4)$$

The first two terms on the right-hand side of Eq. (4) account for the ballistic wave packet propagation, taking explicitly into account the computed *GW*-BSE exciton dispersion via the band velocities $\partial\Omega_{S_B}/\partial\mathbf{Q}$ and effectively coupling spatial and momentum coordinates along the time evolution. The third term, K_{scat}, includes the computed exciton-phonon scattering terms presented above via

$$\begin{aligned} K_{\mathrm{scat}}[n_{S_B}(\mathbf{Q},\mathbf{R})] = &\sum_{\mathbf{q}} k_{S_B(\mathbf{Q}+\mathbf{q})S_B(\mathbf{Q})} n_{S_B}(\mathbf{Q}+\mathbf{q},\mathbf{R}) \\ &- \sum_{\mathbf{q}} k_{S_B(\mathbf{Q})S_B(\mathbf{Q}+\mathbf{q})} n_{S_B}(\mathbf{Q},\mathbf{R}) \\ &- k_{S_B(\mathbf{Q})S_D} n_{S_B}(\mathbf{Q},\mathbf{R}) \\ &- k^{\mathrm{rad}}_{S_B(\mathbf{Q})} n_{S_B}(\mathbf{Q},\mathbf{R})\delta_{\mathbf{Q},\Gamma} \end{aligned} \quad (5)$$

The first two scattering terms denote intraband transitions of the bright exciton, in which the exciton $S_B(\mathbf{Q})$ is respectively created or destroyed. $k_{S_B(\mathbf{Q})S_B(\mathbf{Q}+\mathbf{q})}$ are the weighted scattering rates associated with each momentum-resolved transition summed over all phonon modes, expressed in terms of the scattering rates defined above, $k_{S_B(\mathbf{Q})S_B(\mathbf{Q}+\mathbf{q})} \equiv \Gamma^{S_B S_B}_{\mathbf{q},\mathbf{Q}} = \sum_\nu k_{S_B S_B \nu}(\mathbf{Q},\mathbf{q})$. The third term accounts for exciton decay due to interband scattering into the dark state, with the momentum of all final states summed through $S_D = \sum_{\mathbf{q}} S_D(\mathbf{Q}+\mathbf{q})$, thus $k_{S_B(\mathbf{Q})S_D}$ correspond to the above-defined $\Gamma^{S_B S_D}_{\mathbf{Q}}$. We exclude the reverse process, assuming that dark states go through rapid non-radiative decay (such as coherent coupling to biexciton pairs) before scattering back to a bright state. The last scattering term represents radiative decay from $S_B(\mathbf{Q}=\Gamma)$ to the ground state. We follow Refs. [50,57] and evaluate this term from the exciton oscillator strength and excitation energy (see SM [55])

$$k^{\mathrm{rad}}_{S_B} = \frac{2\pi e^2}{\hbar^2 \mathrm{c}} \frac{\Omega_{S_B(\Gamma)}}{A_{\mathrm{uc}}} \mu_S^2. \quad (6)$$

Here, A_{uc} is the unit cell planar area, $\Omega_{S_B(\Gamma)}$ is the exciton energy at $\mathbf{Q}=\Gamma$, c is the speed of light, and μ_s^2 is the exciton modulus square dipole strength divided by the number of $\mathbf{k}$ points. This leads to a recombination lifetime of ∼3.5 ps, in agreement with previously reported relatively low radiative rates and small radiative signal in pentacene crystals [4,70,71].

Using Eq. (4) we compute the real-time propagation of the photoexcited exciton, starting from an initial Gaussian exciton wave packet [18] centered around the zero momentum and spatial coordinates, with broadening of 2 nm^{-1} and 3 nm in $\mathbf{Q}$ and $\mathbf{R}$ space, respectively. These initial conditions are set to mimic the beam shape of an initial laser excitation. While the spread is considerably smaller than an experimental beam size, it is sufficient to observe the momentum-resolved processes that dominate its early-time evolution in the crystal (see SM for further analysis [55]). Figure 3(a) shows the exciton population following photoexcitation. The initial occupation of the $S_B(\mathbf{Q})$ state, shown schematically in the legend, is classified into $\mathbf{Q}$ points near Γ (yellow, with η defining Γ proximate area; see SM [55]), far from it (blue), and their sum (light blue). Upon interband scattering, a growing occupation of the dark state (gray) accompanies the non-radiative intraband scattering. Radiative recombination is negligible at these timescales. At early times of the exciton evolution, up to 200 fs, the initial population mainly decays via intraband transitions, after which the decay to the S_D state dominates. After 1 ps, the dark state occupies ∼80% of the exciton population.

Figure 3(b) shows the spatial exciton propagation in real space, presented with normalized intensity amplified with respect to the initial time step. (Transitions to the dark state lead to a strong decrease in the non-normalized signal; see SM [55].) The mean squared displacement (MSD) is also shown along the $\hat{\mathbf{x}}$ (purple) and $\hat{\mathbf{y}}$ (teal) directions. At ∼ 100 fs the Gaussian wave packet starts to delocalize

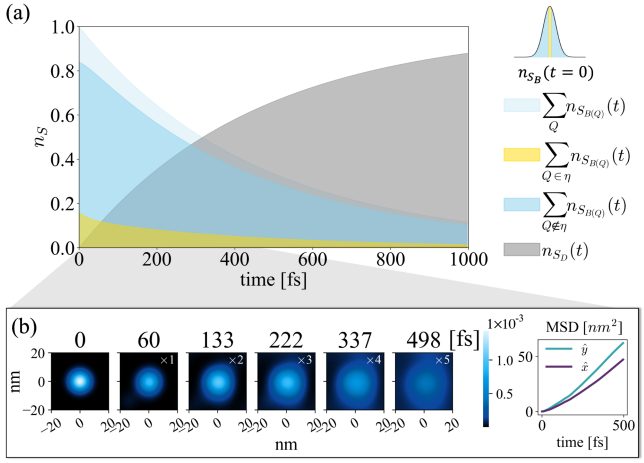

FIG. 3. (a) Exciton wave packet occupation, computed from Eq. (4) for the first 1 ps after excitation, with the scattering rates constructing Fig. 2. The exciton evolution consists of the change in populations of S_B state at $\mathbf{Q} \approx \Gamma$ (within the area η around Γ, yellow), S_B state at the remainder of $\mathbf{Q}$ space (blue), total S_B state population (light blue), and S_D state at all $\mathbf{Q}$ points (gray). (b) Spatial propagation of the wave packet during the first 500 fs. Blue distribution shows the bright state occupation, normalized, and amplified with respect to the initial step. MSD along the $\hat{\mathbf{x}}$ (purple) and $\hat{\mathbf{y}}$ (teal) are shown on the right.

along both the $\hat{\mathbf{x}}$ and $\hat{\mathbf{y}}$ directions. This is an outcome of the exciton LT splitting, as we observed previously for the ballistic regime [18] (see further analysis in the SM [55]). However, unlike in the ballistic regime, the exciton-phonon scattering leads to enhancement of the wave packet broadening, as indicated by the MSD, with preferred directionality of the propagation along $\hat{\mathbf{y}}$ stemming from the nonuniform exciton-phonon scattering. We emphasize that the appearance of anisotropic fast and slow transport axes is a consequence of the anisotropic exciton-phonon coupling and does not appear in the purely ballistic limit [18].

Our calculations reveal three important aspects in the propagation picture. First, the wave packet broadening is anisotropic, directly manifesting the crystal anisotropy through both the LT exciton splitting and phonon scattering, connecting the propagation pattern to the crystal structure. Second, the increase in exciton spread occurs at comparable timescales to dark state occupation, opening the door to tuning the various scattering times via interplay between the bright and dark band alignment. Third, the computed change in the wave packet broadening is nonlinear due to strong coupling between the LT band split and phonon scattering. Still, one can assume linearity for the region above 200 fs, where the ballistic effects reduce and the phonon scattering dominates. At this region we find diffusion coefficients of 0.42 cm^2/s and 0.55 cm^2/s along the $\hat{\mathbf{x}}$ and $\hat{\mathbf{y}}$ directions, respectively. At later times, the occupation of the dark state starts to dominate the exciton transport.

To conclude, we present a theoretical scheme to calculate exciton-phonon interactions and time-resolved exciton evolution in crystals and apply it to study nonradiative processes in crystalline pentacene. Our method supplies a connection between exciton and phonon properties in momentum space and the observed propagation trends in real space, offering a direct relation between crystal structure and transport anisotropy. We find that the excited exciton undergoes intraband scattering (in the bright singlet branch) and interband scattering (into the dark singlet branch) on the same timescale and provide insights into the variety of processes involved. The surprising comparable rates for interband and intraband scattering are facilitated by the band crossing driven by the LT splitting of the bright exciton branch. This band crossing results in complex exciton evolution and manifests in rapid anisotropic exciton wave packet spreading before the occupation of a long-lived dark state. Moreover, the fast population of the dark state elucidates the crucial role of exciton-phonon scattering in nonradiative relaxation pathways in molecular crystals, determining energy transfer efficiency. The rapid interband scattering relies on the relative energy of the bright and dark states and is thus tunable through both crystal packing and molecular composition. Our results shed new light on the role of crystal anisotropy and symmetry at the early stages of exciton transport, setting the stage for a predictive, first-principles description of the underlying dynamical processes dominating efficient energy transfer in organic semiconductors.

We thank Lev Melinkovsky, Mikhail Glazov, Felipe da Jornada, Alexey Chernikov, Andrés Montoya-Castillo, and Aaron Kelly for insightful discussions. G. C. acknowledges the Institute for Environmental Sustainability (IES) Fellowship. D. Y. Q. is supported by the U.S. Department of Energy, Office of Science, Basic Energy Sciences, under Early Career Award No. DE-SC0021965, which provided for the development of the exciton wave packet model. S. R. A. is an incumbent of the Leah Omenn Career Development Chair and acknowledges a Peter and Patricia Gruber Award and an Alon Fellowship. The project has received further funding from the European Research Council (ERC), Grant Agreement No. 101041159, and an Israel Science Foundation Grant No. 1208/19. Development of methods for computing exciton-phonon matrix elements with BerkeleyGW was supported by the Center for Computational Study of Excited-State Phenomena in Energy Materials (C2SEPEM) at Lawrence Berkeley National Laboratory, funded by the U.S. Department of Energy, Office of Science, Basic Energy Sciences, Materials Sciences and Engineering Division, under Contract No. DE-C02-05CH11231. Computational resources were provided by the National Energy Research Scientific Computing Center (NERSC), as well as the ChemFarm local cluster at the Weizmann Institute of Science.

*Corresponding author: diana.qiu@yale.edu
†Corresponding author: sivan.refaely-abramson@weizmann.ac.il

[1] *Fundamentals of Materials for Energy and Environmental Sustainability*, edited by D. S. Ginley and D. Cahen (Cambridge University Press, Cambridge, England, 2011), 10.1017/CBO9780511718786.
[2] *Organic Photovoltaics: Concepts and Realization*, edited by C. J. Brabec, V. Dyakonov, J. Parisi, and N. S. Sariciftci (Springer, Berlin, 2010), 10.1007/978-3-662-05187-0.
[3] L. Kronik and J. B. Neaton, Excited-state properties of molecular solids from first principles, Annu. Rev. Phys. Chem. **67**, 587 (2016).
[4] M. W. B. Wilson, A. Rao, B. Ehrler, and R. H. Friend, Singlet exciton fission in polycrystalline pentacene: From photophysics toward devices, Acc. Chem. Res. **46**, 1330 (2013).
[5] C. Schnedermann, J. Sung, R. Pandya, S. D. Verma, R. Y. S. Chen, N. Gauriot, H. M. Bretscher, P. Kukura, and A. Rao, Ultrafast tracking of exciton and charge carrier transport in optoelectronic materials on the nanometer scale, J. Phys. Chem. Lett. **10**, 6727 (2019).
[6] S. R. Yost, J. Lee, M. W. B. Wilson, T. Wu, D. P. McMahon, R. R. Parkhurst, N. J. Thompson, D. N. Congreve, A. Rao, K. Johnson, M. Y. Sfeir, M. G. Bawendi, T. M. Swager, R. H. Friend, M. A. Baldo, and T. V. Voorhis, A transferable model for singlet-fission kinetics, Nat. Chem. **6**, 492 (2014).
[7] A. Rao and R. H. Friend, Harnessing singlet exciton fission to break the Shockley–Queisser limit, Nat. Rev. Mater. **2**, 17063 (2017).
[8] D. Casanova, Theoretical modeling of singlet fission, Chem. Rev. **118**, 7164 (2018).
[9] T. Zhu and L. Huang, Exciton transport in singlet fission materials: A new hare and tortoise story, J. Phys. Chem. Lett. **9**, 6502 (2018).
[10] S. Sharifzadeh, Many-body perturbation theory for understanding optical excitations in organic molecules and solids, J. Phys. Condens. Matter **30**, 153002 (2018).
[11] T. Zhu, Y. Wan, and L. Huang, Direct imaging of Frenkel exciton transport by ultrafast microscopy, Acc. Chem. Res. **50**, 1725 (2017).
[12] N. S. Ginsberg and W. A. Tisdale, Spatially resolved photogenerated exciton and charge transport in emerging semiconductors, Annu. Rev. Phys. Chem. **71**, 1 (2020).
[13] Y. Wan, Z. Guo, T. Zhu, S. Yan, J. Johnson, and L. Huang, Cooperative singlet and triplet exciton transport in tetracene crystals visualized by ultrafast microscopy, Nat. Chem. **7**, 785 (2015).
[14] S. Refaely-Abramson, F. H. da Jornada, S. G. Louie, and J. B. Neaton, Origins of singlet fission in solid pentacene from an *ab initio* Green's function approach, Phys. Rev. Lett. **119**, 267401 (2017).
[15] C. Cocchi, T. Breuer, G. Witte, and C. Draxl, Polarized absorbance and Davydov splitting in bulk and thin-film pentacene polymorphs, Phys. Chem. Chem. Phys. **20**, 29724 (2018).
[16] A. R. Altman, S. Refaely-Abramson, and F. H. da Jornada, Identifying hidden intracell symmetries in molecular crystals and their impact for multiexciton generation, J. Phys. Chem. Lett. **13**, 747 (2022).
[17] B. D. Folie, J. B. Haber, S. Refaely-Abramson, J. B. Neaton, and N. S. Ginsberg, Long-lived correlated triplet pairs in a π stacked crystalline pentacene derivative, J. Am. Chem. Soc. **140**, 2326 (2018).
[18] D. Y. Qiu, G. Cohen, D. Novichkova, and S. Refaely-Abramson, Signatures of dimensionality and symmetry in exciton band structure: Consequences for exciton dynamics and transport, Nano Lett. **21**, 7644 (2021).
[19] R. Schuster, M. Knupfer, and H. Berger, Exciton band structure of pentacene molecular solids: Breakdown of the Frenkel exciton model, Phys. Rev. Lett. **98**, 037402 (2007).
[20] S. Sharifzadeh, P. Darancet, L. Kronik, and J. B. Neaton, Low-energy charge-transfer excitons in organic solids from first-principles: The case of pentacene, J. Phys. Chem. Lett. **4**, 2197 (2013).
[21] N. Monahan and X.-Y. Zhu, Charge transfer–mediated singlet fission, Annu. Rev. Phys. Chem. **66**, 601 (2015).
[22] T. C. Berkelbach, M. S. Hybertsen, and D. R. Reichman, Microscopic theory of singlet exciton fission. III. Crystalline pentacene, J. Chem. Phys. **141**, 074705 (2014).
[23] J. Aragó and A. Troisi, Dynamics of the excitonic coupling in organic crystals, Phys. Rev. Lett. **114**, 026402 (2015).
[24] B. K. Chang, J.-J. Zhou, N.-E. Lee, and M. Bernardi, Intermediate polaronic charge transport in organic crystals from a many-body first-principles approach, npj Comput. Mater. **8**, 63 (2022).
[25] H. Seiler, M. Krynski, D. Zahn, S. Hammer, Y. W. Windsor, T. Vasileiadis, J. Pflaum, R. Ernstorfer, M. Rossi, and H. Schwoerer, Nuclear dynamics of singlet exciton fission in pentacene single crystals, Sci. Adv. **7**, eabg0869 (2021).
[26] A. M. Alvertis, R. Pandya, L. A. Muscarella, N. Sawhney, M. Nguyen, B. Ehrler, A. Rao, R. H. Friend, A. W. Chin, and B. Monserrat, Impact of exciton delocalization on exciton-vibration interactions in organic semiconductors, Phys. Rev. B **102**, 081122(R) (2020).
[27] T. C. Berkelbach, Electronic structure and dynamics of singlet fission in organic molecules and crystals, Adv. Chem. Phys. **162**, 1 (2017).
[28] W. Kohn and L. J. Sham, Self-consistent equations including exchange and correlation effects, Phys. Rev. **140**, A1133 (1965).
[29] M. S. Hybertsen and S. G. Louie, Electron correlation in semiconductors and insulators: Band gaps and quasiparticle energies, Phys. Rev. B **34**, 5390 (1986).
[30] M. Rohlfing and S. G. Louie, Electron-hole excitations and optical spectra from first principles, Phys. Rev. B **62**, 4927 (2000).
[31] S. Sharifzadeh, A. Biller, L. Kronik, and J. B. Neaton, Quasiparticle and optical spectroscopy of the organic semiconductors pentacene and PTCDA from first principles, Phys. Rev. B **85**, 125307 (2012).
[32] P. Cudazzo, M. Gatti, A. Rubio, and F. Sottile, Frenkel versus charge-transfer exciton dispersion in molecular crystals, Phys. Rev. B **88**, 195152 (2013).
[33] P. B. Coto, S. Sharifzadeh, J. B. Neaton, and M. Thoss, Low-lying electronic excited states of pentacene oligomers: A comparative electronic structure study in the context of singlet fission, J. Chem. Theory Comput. **11**, 147 (2015).
[34] S. Refaely-Abramson, M. Jain, S. Sharifzadeh, J. B. Neaton, and L. Kronik, Solid-state optical absorption from optimally

tuned time-dependent range-separated hybrid density functional theory, Phys. Rev. B **92**, 081204(R) (2015).
[35] T. Rangel, K. Berland, S. Sharifzadeh, F. Brown-Altvater, K. Lee, P. Hyldgaard, L. Kronik, and J. B. Neaton, Structural and excited-state properties of oligoacene crystals from first principles, Phys. Rev. B **93**, 115206 (2016).
[36] D. Y. Qiu, T. Cao, and S. G. Louie, Nonanalyticity, valley quantum phases, and lightlike exciton dispersion in monolayer transition metal dichalcogenides: Theory and first-principles calculations, Phys. Rev. Lett. **115**, 176801 (2015).
[37] P. Cudazzo, L. Sponza, C. Giorgetti, L. Reining, F. Sottile, and M. Gatti, Exciton band structure in two-dimensional materials, Phys. Rev. Lett. **116**, 066803 (2016).
[38] P. Cudazzo, F. Sottile, A. Rubio, and M. Gatti, Exciton dispersion in molecular solids, J. Phys. Condens. Matter **27**, 113204 (2015).
[39] F. Giustino, Electron-phonon interactions from first principles, Rev. Mod. Phys. **89**, 015003 (2017).
[40] M. Zacharias and F. Giustino, One-shot calculation of temperature-dependent optical spectra and phonon-induced band-gap renormalization, Phys. Rev. B **94**, 075125 (2016).
[41] T. A. Huang, M. Zacharias, D. K. Lewis, F. Giustino, and S. Sharifzadeh, Exciton–phonon interactions in monolayer germanium selenide from first principles, J. Phys. Chem. Lett. **12**, 3802 (2021).
[42] H.-Y. Chen, D. Sangalli, and M. Bernardi, Exciton-phonon interaction and relaxation times from first principles, Phys. Rev. Lett. **125**, 107401 (2020).
[43] F. Paleari, H. P. C. Miranda, A. Molina-Sánchez, and L. Wirtz, Exciton-phonon coupling in the ultraviolet absorption and emission spectra of bulk hexagonal boron nitride, Phys. Rev. Lett. **122**, 187401 (2019).
[44] E. Cannuccia, B. Monserrat, and C. Attaccalite, Theory of phonon-assisted luminescence in solids: Application to hexagonal boron nitride, Phys. Rev. B **99**, 081109(R) (2019).
[45] G. Antonius and S. G. Louie, Theory of exciton-phonon coupling, Phys. Rev. B **105**, 085111 (2022).
[46] X.-W. Zhang and T. Cao, *Ab initio* calculations of spin-nonconserving exciton–phonon scattering in monolayer transition metal dichalcogenides, J. Phys. Condens. Matter **34**, 264002 (2022).
[47] Y.-H. Chan, J. B. Haber, M. H. Naik, J. Neaton, D. Y. Qiu, F. H. da Jornada, and S. G. Louie, Exciton lifetime and optical linewidth profile via exciton-phonon interactions: Theory and first-principles calculations for monolayer MoS_2, Nano Lett. **23**, 3971 (2023).
[48] A. M. Alvertis, J. B. Haber, E. A. Engel, S. Sharifzadeh, and J. B. Neaton, Phonon-induced localization of excitons in molecular crystals from first principles, Phys. Rev. Lett. **130**, 086401 (2023).
[49] J. Deslippe, G. Samsonidze, D. A. Strubbe, M. Jain, M. L. Cohen, and S. G. Louie, BerkeleyGW: A massively parallel computer package for the calculation of the quasiparticle and optical properties of materials and nanostructures, Comput. Phys. Commun. **183**, 1269 (2012).
[50] H.-Y. Chen, V. A. Jhalani, M. Palummo, and M. Bernardi, *Ab initio* calculations of exciton radiative lifetimes in bulk crystals, nanostructures, and molecules, Phys. Rev. B **100**, 075135 (2019).
[51] G. M. Akselrod, P. B. Deotare, N. J. Thompson, J. Lee, W. A. Tisdale, M. A. Baldo, V. M. Menon, and V. Bulović, Visualization of exciton transport in ordered and disordered molecular solids, Nat. Commun. **5**, 3646 (2014).
[52] M. Delor, H. L. Weaver, Q. Yu, and N. S. Ginsberg, Imaging material functionality through three-dimensional nanoscale tracking of energy flow, Nat. Mater. **19**, 56 (2020).
[53] R. Pandya, A. M. Alvertis, Q. Gu, J. Sung, L. Legrand, D. Kréher, T. Barisien, A. W. Chin, C. Schnedermann, and A. Rao, Exciton diffusion in highly-ordered one dimensional conjugated polymers: Effects of back-bone torsion, electronic symmetry, phonons and annihilation, J. Phys. Chem. Lett. **12**, 3669 (2021).
[54] T. Siegrist, C. Besnard, S. Haas, M. Schiltz, P. Pattison, D. Chernyshov, B. Batlogg, and C. Kloc, A polymorph lost and found: The high-temperature crystal structure of pentacene, Adv. Mater. **19**, 2079 (2007).
[55] See Supplemental Material at http://link.aps.org/supplemental/10.1103/PhysRevLett.132.126902 for more elaborate details about the method development and computational details, which includes Refs. [14,18,29,30, 49,50,54,56–62].
[56] E. M. Lifshitz and L. P. Pitaevski, Chapter I—kinetic theory of gases, physical kinetics, in *Course of Theoretical Physics* (Elsevier Ltd,, 1981), pp. 1–88, 10.1016/B978-0-08-026480-6.50006-0.
[57] C. D. Spataru, S. Ismail-Beigi, R. B. Capaz, and S. G. Louie, Theory and *ab initio* calculation of radiative lifetime of excitons in semiconducting carbon nanotubes, Phys. Rev. Lett. **95**, 247402 (2005).
[58] P. Giannozzi *et al.*, Quantum espresso: A modular and open-source software project for quantum simulations of materials, J. Phys. Condens. Matter **21**, 395502 (2009).
[59] https://summary.ccdc.cam.ac.uk.
[60] J. P. Perdew, K. Burke, and M. Ernzerhof, Generalized gradient approximation made simple, Phys. Rev. Lett. **77**, 3865 (1996).
[61] S. Poncé, E. R. Margine, C. Verdi, and F. Giustino, Epw: Electron–phonon coupling, transport and superconducting properties using maximally localized Wannier functions, Comput. Phys. Commun. **209**, 116 (2016).
[62] D. Nabok, P. Puschnig, C. Ambrosch-Draxl, O. Werzer, R. Resel, and Detlef-M. Smilgies, Crystal and electronic structures of pentacene thin films from grazing-incidence x-ray diffraction and first-principles calculations, Phys. Rev. B **76**, 235322 (2007).
[63] L. C. Andreani, F. Bassani, and A. Quattropani, Longitudinal-transverse splitting in Wannier excitons and polariton states, Il Nuovo Cimento D **10**, 1473 (1988).
[64] M. M. Denisov and V. P. Makarov, Longitudinal and transverse excitons in semiconductors, Phys. Status Solidi B **56**, 9 (1973).
[65] V. M. Agranovich and V. L. Ginzburg, *Spatial Dispersion in Crystal Optics and the Theory of Excitons* (Interscience Publishers, London, New York, 1966).
[66] F. Brown-Altvater, T. Rangel, and J. B. Neaton, *Ab initio* phonon dispersion in crystalline naphthalene using van der Waals density functionals, Phys. Rev. B **93**, 195206 (2016).

[67] H.-G. Duan, A. Jha, X. Li, V. Tiwari, H. Ye, P. K. Nayak, X.-L. Zhu, Z. Li, T. J. Martinez, M. Thorwart, and R. J. D. Miller, Intermolecular vibrations mediate ultrafast singlet fission, Sci. Adv. **6**, eabb0052 (2020).

[68] A. A. Bakulin, S. E. Morgan, T. B. Kehoe, M. W. Wilson, A. W. Chin, D. Zigmantas, D. Egorova, and A. Rao, Real-time observation of multiexcitonic states in ultrafast singlet fission using coherent 2D electronic spectroscopy, Nat. Chem. **8**, 16 (2016).

[69] A. Neef, S. Beaulieu, S. Hammer, S. Dong, J. Maklar, T. Pincelli, R. P. Xian, M. Wolf, L. Rettig, J. Pflaum, and R. Ernstorfer, Orbital-resolved observation of singlet fission, Nature (London) **616**, 275 (2023).

[70] C. Jundt, G. Klein, B. Sipp, J. L. Moigne, M. Joucla, and A. Villaeys, Exciton dynamics in pentacene thin films studied by pump-probe spectroscopy, Chem. Phys. Lett. **241**, 84 (1995).

[71] H. Marciniak, M. Fiebig, M. Huth, S. Schiefer, B. Nickel, F. Selmaier, and S. Lochbrunner, Ultrafast exciton relaxation in microcrystalline pentacene films, Phys. Rev. Lett. **99**, 176402 (2007).